Thermal evolution of Mercury as constrained by MESSENGER observations

Nathalie C. Michel,[1] Steven A. Hauck II,[1] Sean C. Solomon,[2,3] Roger J. Phillips,[4] James H. Roberts,[5] and Maria T. Zuber[6]

Received 22 June 2012; revised 20 December 2012; accepted 28 December 2012; published 22 May 2013.

[1] Orbital observations of Mercury by the MErcury Surface, Space ENvironment, GEochemistry, and Ranging (MESSENGER) spacecraft provide new constraints on that planet's thermal and interior evolution. Specifically, MESSENGER observations have constrained the rate of radiogenic heat production via measurement of uranium, thorium, and potassium at the surface, and identified a range of surface compositions consistent with high-temperature, high-degree partial melts of the mantle. Additionally, MESSENGER data have placed new limits on the spatial and temporal variation in volcanic and tectonic activity and enabled determination that the planet's core is larger than previously estimated. Because Mercury's mantle layer is also thinner than previously thought, this result gives greater likelihood to the possibility that mantle convection is marginally supercritical or even that the mantle is not convecting. We simulate mantle convection and magma generation within Mercury's mantle under two-dimensional axisymmetry and a broad range of conditions to understand the implications of MESSENGER observations for the thermal evolution of the planet. These models demonstrate that mantle convection can persist in such a thin mantle for a substantial portion of Mercury's history, and often to the present, as long as the mantle is thicker than ~300 km. We also find that magma generation in Mercury's convecting mantle is capable of producing widespread magmas by large-degree partial melting, consistent with MESSENGER observations of the planet's surface chemistry and geology.

Citation: Michel, N. C., S. A. Hauck II, S. C. Solomon, R. J. Phillips, J. H. Roberts, and M. T. Zuber (2013), Thermal evolution of Mercury as constrained by MESSENGER observations, *J. Geophys. Res. Planets*, *118*, 1033–1044, doi:10.1002/jgre.20049.

1. Introduction

[2] The evolution of a planetary body is fundamentally intertwined with the transport and loss of heat from its interior [*Stevenson et al.*, 1983]. Planetary heat loss is a dynamic process controlled by the internal structure and composition of a body and its dominant mode of heat transfer, and has consequences for the history of surface volcanic and tectonic activity and magnetic field generation. Understanding the thermal evolution of a planetary body, therefore, provides crucial context for interpreting a planet's geological history [e.g., *Schubert et al.*, 2001]. Recent orbital observations of Mercury by the MErcury Surface, Space ENvironment, GEochemistry, and Ranging (MESSENGER) spacecraft provide new constraints on that planet's geological, geochemical, and geophysical history, and therefore its internal evolution as well.

[3] The Mariner 10 flybys of Mercury in 1974 and 1975 confirmed the planet's high bulk density of 5430 kg m^{-3} [*Anderson et al.*, 1987], which has long suggested a relatively large metallic core [e.g., *Solomon*, 1976, 1977], implying a thin silicate shell no thicker than about 600 km [e.g., *Spohn et al.*, 2001; *Harder and Schubert*, 2001; *Van Hoolst et al.*, 2007]. One of the notable aspects of previous studies of Mercury's thermal evolution is a lack of agreement as to whether Mercury's mantle is likely to be actively convecting at present [e.g., *Breuer et al.*, 2007]. Indeed, some workers found that for models with temperature- and pressure-dependent, non-Newtonian rheology and crustal formation, mantle convection was confined only to the early stages of evolution and marked by extensive melting and differentiation [e.g., *Solomatov and Reese*, 2001; *Hauck et al.*, 2004]. At some later time convection and melting ceased in such models, and the planet cooled in a conductive regime. However, *Redmond and King* [2007] demonstrated with two-dimensional (2-D) simulations that mantle

Additional supporting information may be found in the online version of this article.

[1]Department of Earth, Environmental, and Planetary Sciences, Case Western Reserve University, Cleveland, Ohio, USA.
[2]Department of Terrestrial Magnetism, Carnegie Institution of Washington, Washington, D.C., USA.
[3]Lamont-Doherty Earth Observatory, Columbia University, Palisades, New York, USA.
[4]Planetary Science Directorate, Southwest Research Institute, Boulder, Colorado, USA.
[5]Space Department, The Johns Hopkins University Applied Physics Laboratory, Laurel, Maryland, USA.
[6]Department of Earth, Atmospheric and Planetary Sciences, Massachusetts Institute of Technology, Cambridge, Massachusetts, USA.

Corresponding author: N. C. Michel, Department of Earth, Environmental, and Planetary Sciences, Case Western Reserve University, Cleveland, OH, 44106, USA. (nathalie.michel@case.edu)

2169-9097/13/10.1002/jgre.20049

convection can persist over Mercury's lifetime, albeit at modest Rayleigh numbers relative to those of the larger terrestrial planets, under a range of combinations of internal heating rate and core heat flux. In three-dimensional (3-D) simulations, *King* [2008] similarly found models in which modern convection is ongoing. *Redmond and King* [2007] and *King* [2008] reached a different conclusion from that of *Hauck et al.* [2004] regarding the status of present convection because of differences in the cooling histories among models. More recently, *Grott et al.* [2011] investigated the role of a near-surface, thermally insulating regolith and found slower planetary cooling and persistent mantle convection, even for a relatively large fractional core radius.

[4] Throughout its first year of orbital observations, MESSENGER's measurements have yielded many discoveries that bear on the thermal and interior evolution of Mercury. Indeed, MESSENGER images and topographic measurements have documented evidence for both widespread plains volcanism [*Denevi et al.*, 2009; *Head et al.*, 2011] and substantial changes to long-wavelength topography since the end of late heavy bombardment of the inner solar system [*Zuber et al.*, 2012; *Balcerski et al.*, 2012; *Solomon et al.*, 2012], indicative of a dynamic geological and internal history. The spacecraft has also measured the abundances of many major elements at the surface, providing constraints on magma compositions [*Nittler et al.*, 2011] and the abundances of long-lived radioactive elements that provide limits on the history of heat production on Mercury [*Peplowski et al.*, 2011]. MESSENGER's magnetic field investigations have confirmed the presence of Mercury's predominantly dipolar internal magnetic field, while revealing that this field is axially symmetric but strongly asymmetric about the planet's geographic equator [*Anderson et al.*, 2011]. Finally, observations of Mercury's orbital and spin dynamics [*Margot et al.*, 2007, 2012] and improved knowledge of the planet's gravity field have allowed the determination of the planet's dimensionless polar moment of inertia (C/Mr_p^2), where M and r_p are Mercury's mass and radius, respectively, as well as the ratio of the moment of inertia of the outer solid shell to the planetary moment of inertia (C_m/C) [*Smith et al.*, 2012; *Margot et al.*, 2012]. These parameters confirm that Mercury has a large core with the top of its fluid layer at only ~400 km depth [*Smith et al.*, 2012; *Hauck et al.*, 2012].

[5] The thermal evolution of Mercury is controlled by the heat transport processes of conduction and convection in the mantle. Under conduction, heat is transported via diffusion, which tends to be less efficient than advective transport during convection. However, Mercury's thin mantle implies that its Rayleigh number (*Ra*), the ratio between buoyancy forces and viscous dissipation that describes the vigor of convection, may be low because *Ra* scales as the third power of the thickness of the convecting layer. As a consequence, Mercury's mantle may be only marginally unstable to convection, or it may even be stable if the Rayleigh number is below its critical value, Ra_c [e.g., *Schubert et al.*, 2001].

[6] In this paper, we reexamine the question of Mercury's long-term thermal evolution because it is now constrained by new observations from MESSENGER. The goal here is to address two major aspects of Mercury's thermal evolution: the longevity of convection within the mantle and the implications of widespread volcanism early in the planet's history.

2. Method

2.1. Model

[7] To study the thermal evolution of Mercury, we employed the finite element mantle convection code Citcom in axisymmetric spherical shell geometry [*Moresi and Solomatov*, 1995; *Roberts and Zhong*, 2004] modified to account for secular cooling of the core [*Michel and Forni*, 2011]. The axisymmetric spherical shell geometry is well suited to modeling the global thermal evolution of Mercury in a computationally efficient manner without resorting to one-dimensional energy balance, as in parameterized convection models [e.g., *Schubert et al.*, 1988; *Hauck et al.*, 2004; *Grott et al.*, 2011]. The convection is described by the equations of conservation of mass, momentum and energy, under the assumptions of incompressibility and the extended Boussinesq approximation [*Christensen and Yuen*, 1985; *Christensen*, 1995]. The dimensionless governing equations are

$$\nabla\cdot\mathbf{u} = 0 \tag{1}$$

$$-\nabla P + \nabla\cdot\left[\eta\left(\nabla\mathbf{u} + \nabla^T\mathbf{u}\right)\right] + Ra\, T\, \mathbf{e_r} = 0 \tag{2}$$

$$\frac{\partial T}{\partial t} + \mathbf{u}\cdot\nabla T + Di\, \mathbf{u_r}\, T + \left(\frac{Di}{Ra}\right)\boldsymbol{\sigma}\cdot\nabla\mathbf{u} - \nabla^2 T = H_{TOT} \tag{3}$$

[8] The equations of conservation of (1) mass and (2) momentum determine the velocity field $\mathbf{u}$, and the conservation of energy (3) provides the temperature T in the mantle. Here P is the dynamic pressure, η is the viscosity, $\mathbf{e_r}$ is a unit vector in the radial direction, $\boldsymbol{\sigma}$ is the deviatoric stress tensor, and H_{TOT} is the energy from internal heat production due to radioactive decay. The third term in equation (3) accounts for adiabatic heating, the fourth term tracks any heat generated by viscous dissipation, and the fifth term is related to heat conduction. The dimensionless Rayleigh number *Ra* and dissipation number *Di* are respectively defined by

$$Ra = \frac{\alpha\rho g \Delta T {r_p}^3}{\kappa\eta_1} \tag{4}$$

$$Di = \frac{\alpha g r_p}{C_p} \tag{5}$$

where α is the volumetric coefficient of thermal expansion, ρ the mean density, g the gravitational acceleration, ΔT the temperature difference between the top and bottom boundaries of the spherical shell being modeled, κ the thermal diffusivity, C_p the heat capacity, η_1 the reference viscosity defined at the bottom of the shell, and r_p is the radius of the planet. Because we use the length scale r_p in all nondimensionalization, rather than the thickness of the convecting mantle d, the Rayleigh numbers in the present work are larger by a factor $(r_p/d)^3$ than in convection studies that invoke scaling by d.

[9] An important contribution to the thermal evolution of the mantle of a planet is the cooling of the core. We have accounted for the overall cooling of the core by parameterizing the core-mantle boundary (CMB) temperature as a function of time by means of a core energy balance for secular cooling [*Michel and Forni*, 2011]. Core cooling and the release of latent heat and gravitational potential energy due

to solidification of core material are substantial contributors to the internal evolution of a planet, particularly one with a relatively large core [e.g., *Stevenson et al*., 1983; *Schubert et al*., 1988]. However, observations of Mercury's surface composition imply that Mercury formed from strongly chemically reduced precursory material [*Nittler et al*., 2011], which suggests that contrary to a common prior presumption [e.g., *Schubert et al*., 1988; *Hauck et al*., 2004; *Breuer et al*., 2007; *Williams et al*., 2007; *Grott et al*., 2011], the planet's core may not be dominated by a binary alloy of iron and sulfur. Rather, under strongly reducing conditions, silicon will partition into the metal phase [e.g., *McCoy et al*., 1999; *Malavergne et al*., 2010], and the core may be just as, or more, likely to be composed of an iron-silicon alloy or an iron-sulfur-silicon alloy [e.g., *Smith et al*., 2012; *Hauck et al*., 2012]. Unfortunately, the high-pressure phase relationships for these materials are not nearly as well constrained as those for the iron-sulfur system. Therefore, we have focused only on the effects of secular cooling of the core following *Stevenson et al*. [1983], and in effect we underestimate the amount of heat supplied to the mantle by the core in cases where core solidification is thermodynamically favored. The energy balance for the core is defined by

$$\frac{\mathrm{d}T_{\mathrm{cmb}}}{\mathrm{d}t} = -\frac{S_{\mathrm{c}}}{\rho_{\mathrm{c}} C_{\mathrm{c}} V_{\mathrm{c}} \varepsilon_{\mathrm{c}}} F_{\mathrm{c}}(t) \tag{6}$$

where T_{cmb} is the temperature at the CMB, S_{c} is the core surface area, ρ_{c} the density of core material, C_{c} the heat capacity of core material, V_{c} the core volume, ε_{c} a constant that relates the average core temperatures to that at the core-mantle boundary, and F_{c} the heat flux from the core.

[10] We have assumed that the viscosity structure of Mercury's mantle depends on both temperature and depth. The equation that describes the variation of viscosity within the model is derived from the Arrhenius law [*Davaille and Jaupart*, 1994] and is written with nondimensional variables as

$$\eta = \eta_0 \exp\left[\frac{E^* + Z^*\left(r_{\mathrm{p}}^* - r^*\right)}{T^* + T_{\mathrm{S}}^*} - \frac{E^* + Z^*\left(r_{\mathrm{p}}^* - r_{\mathrm{c}}^*\right)}{1.0 + T_{\mathrm{S}}^*}\right] \tag{7}$$

where E is the activation energy for viscous deformation, Z the activation volume, r the radius, and r_{c} the core radius. Starred quantities denote nondimensional values [*Zhong et al*., 2000; *Roberts and Zhong*, 2006].T_{S}^* is defined by

$$T_{\mathrm{S}}^* = \frac{T_0}{T_{\mathrm{cmb}} - T_0} \tag{8}$$

where T_0 is the surface temperature. When the viscosity contrast between the CMB (η_1) and the surface (η_0) is sufficiently high, a thick stagnant layer is formed near the top boundary [e.g., *Solomatov*, 1995].

[11] An approximate, single exponential function has been used to describe the decay of radioactive elements in the mantle:

$$Q(t) = Q_0 \exp(-\lambda t) \tag{9}$$

where Q_0 is the initial heat production in the mantle and λ the mean decay constant of radioactive elements derived from the relative amounts of U, K, and Th determined from MESSENGER Gamma-Ray Spectrometer (GRS) measurements of Mercury's surface composition.

[12] Our finite element mesh employed an array of 65 radial by 257 azimuthal elements that was refined near the inner boundary of the shell to improve determination of the heat flux at the core-mantle boundary. Isothermal temperature and free-slip velocity boundary conditions were applied at the top of the shell. Free-slip or no-slip velocity boundary conditions were applied at the bottom of the shell depending on the conditions of each case studied. Finally, laterally homogeneous but time-varying temperatures were imposed at the core-mantle boundary.

2.2. Approach

[13] We investigate Mercury's thermal evolution by conducting a series of 2-D axisymmetric numerical mantle convection simulations guided by new observations from MESSENGER where possible (e.g., the abundances of heat-producing elements) and exploring a broad range of values for parameters that are weakly constrained (e.g., mantle rheology). We considered and compared the consequences of different mantle rheologies, absolute heat production, bottom velocity boundary conditions, and initial conditions for a range of core radii (1800–2100 km). The goal of this work is to understand the conditions and periods over which Mercury's mantle has been dynamically active and capable of producing widespread volcanism.

[14] MESSENGER provides important constraints on the surface composition of Mercury that in turn affords us the first crucial clues to the more elusive question of the composition of the mantle. From X-ray fluorescence measurements it appears that surface compositions are broadly consistent with rock types intermediate between magnesian basalts and more ultramafic compositions similar to terrestrial komatiites [*Nittler et al*., 2011; *Charlier et al*., 2012; *Stockstill-Cahill et al*., 2012]. Rocks of these compositions may be consistent with a peridotitic or even a more pyroxene-rich source, and therefore we consider a range of reference viscosities for the mantle bounded by values appropriate for dry olivine [e.g., *Karato and Wu*, 1993] and dry enstatite [*Mackwell*, 1991]. Although dislocation creep might be more efficient than diffusion creep [e.g., *Karato and Wu*, 1993; *Reese et al*., 1998], on the basis of previous work [e.g., *Hauck and Phillips*, 2002], the difference between these two mechanisms is expected to be minor for overall thermal evolution. Hence, we focused our modeling on diffusion creep. The reference viscosity varies in our models from 10^{19} Pa s to 10^{21} Pa s, and we considered a range of initial CMB temperatures from 1700 to 2300 K.

[15] Furthermore, in our models the internal heat production declines at a rate consistent with the ratios of long-lived radioisotopes in Mercury's surface materials as measured by MESSENGER's GRS [*Peplowski et al*., 2011]. Data from the GRS indicate average surface abundances of 1150 ± 220 ppm for potassium (K), 220 ± 60 ppb for thorium (Th), and 90 ± 20 ppb for uranium (U) [*Peplowski et al*., 2011]. Although the partitioning of heat-producing elements between the crust and mantle is weakly constrained, the abundances of radioactive elements in the mantle are likely smaller than the surface abundances because U, K, and Th tend to be concentrated in surface rocks due their highly incompatible nature during partial melting. Therefore, we considered a

broad range of absolute heat production for the mantle (Figure 1) ranging from 10% to 90% of that implied by surface abundances.

[16] Typical parameters fixed for all models and their nominal values for the mantle convection simulations are listed in Table 1, and variable parameters are indicated in Table 2. A detailed description of all the models can also be found in Tables S1 and S2 in the Supporting Information. The importance of the temperature dependence of the mantle thermal conductivity and the insulating effect of a low-conductivity crust have been demonstrated for the thermal evolution of Mars [*Hauck and Phillips*, 2002; *Grott and Breuer*, 2007] and Mercury [*Grott et al*., 2011]. For the sake of computational simplicity, we employ a constant thermal conductivity throughout our models. Rather than use the commonly assumed value of $4\,W\,m^{-1}\,K^{-1}$ for thermal conductivity, we approximated the role of a lower-conductivity crust and a mantle for which the thermal conductivity is lower because of the temperature-dependence of thermal conductivity by adopting an average conductivity k for the combined silicate layer of $3\,W\,m^{-1}\,K^{-1}$. The thermal evolution of a planet is particularly sensitive to the thermal diffusivity, which controls the rate of conductive cooling through the lid. Differences in that parameter are the major reason that the models of *Grott et al*. [2011] are more prone to long-lived mantle convection than those of *Hauck et al*. [2004], which utilized a value for k of $4\,W\,m^{-1}\,K^{-1}$. However, the choice of conductivity between 3 and $4\,W\,m^{-1}\,K^{-1}$ has a rather modest effect on mantle convection relative to the uncertainty in mantle viscosity. Indeed, we find in test cases that models with $k = 3\,W\,m^{-1}\,K^{-1}$ tend to have mantle convection persisting only slightly longer (less than 1 Gy) than those with $k = 4\,W\,m^{-1}\,K^{-1}$. The mantle density has been taken equal to $3500\,kg\,m^{-3}$, so the thermal diffusivity is equal to $7 \times 10^{-7}\,m^2\,s^{-1}$.

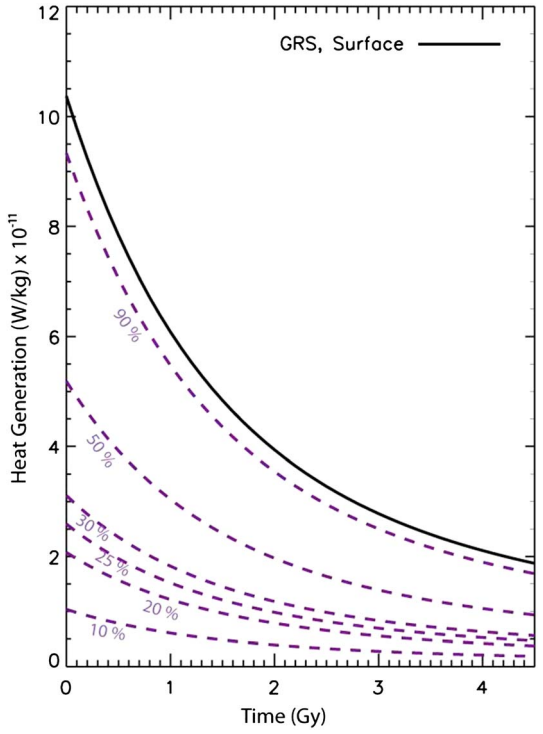

Figure 1. Heat generation per unit mass in the bulk silicate fraction of Mercury over the past 4.5 Gy, from *Peplowski et al*. [2011]. Purple dashed lines correspond to the mantle heat production included in our simulations and shown as a fraction of the surface heat production inferred from surface abundance measurements.

Table 1. Parameters Fixed for All Simulations

Parameter	Symbol	Value	Units
Radius of the planet	r_p	2440	km
Density of the mantle	ρ_m	3500	$kg\,m^{-3}$
Heat capacity of the mantle	C_p	1212	$J\,kg^{-1}\,K^{-1}$
Mantle thermal diffusivity	κ	7×10^{-7}	$m^2\,s^{-1}$
Mantle thermal conductivity	k	3	$W\,m^{-1}\,K^{-1}$
Thermal expansivity	α	3×10^{-5}	K^{-1}
Surface temperature	T_0	401	K
Non-dimensional initial interior temperature	T_i	0.95	-
Surface gravitational acceleration	g	3.76	$m\,s^{-2}$
Constant relating CMB to mean core temperature	ε_c	1.1	
Activation energy	E	300	$kJ\,mol^{-1}$
Activation volume	Z	6	$cm^3\,mol^{-1}$

Table 2. Parameters Varied Among Simulations

Parameter	Range of Value	Units
Initial CMB temperature	1700–2300	K
Initial reference viscosity	10^{19}–10^{21}	Pa s
Initial Rayleigh number	10^7–2×10^9	-
Initial mantle heat production	0–8.6×10^{-11}	$W\,kg^{-1}$

[17] We considered two surface temperature boundary conditions. Mercury experiences an extraordinary range of surface temperatures as an airless body in a 3:2 spin-orbit resonance with, and in close proximity to, the Sun [e.g., *Vasavada et al*., 1999]. Therefore, we explored the effects of variable surface temperatures, focusing on the latitudinal variations consistent with our axisymmetric model. These models employ surface temperatures that vary with latitude at values appropriate for approximately 0.5 m below the surface (below the diurnal wave) computed along a line of longitude through Mercury's hot poles (i.e., 0° and 180° longitude) [*Vasavada et al*., 1999; *Williams et al*., 2011]. To facilitate intercomparison with these earlier models, we also considered a constant surface temperature of 401 K, the average of the latitudinally variable surface temperature, rather than the commonly used value of 440 K [e.g., *Turcotte and Schubert*, 2002; *Hauck et al*., 2004; *Breuer et al*., 2007; *Redmond and King*, 2007; *Grott et al*., 2011].

[18] Multiple measures of the internal structure of Mercury have been determined from the MESSENGER-derived values for two of the second-degree coefficients in the spherical harmonic expansion of Mercury's gravity field (C_{20} and C_{22}) [*Smith et al*., 2012] and several years of Earth-based radar measurements of Mercury's obliquity and the amplitude of its forced libration [*Margot et al*., 2007, 2012]. The normalized polar moment of inertia, C/Mr_p^2, and the fractional polar moment of the outermost solid shell of the planet, C_m/C, are found to be 0.346 ± 0.014 and 0.431 ± 0.025, respectively [*Margot*

et al., 2012; *Hauck et al*., 2012]. These values are somewhat smaller than reported by *Smith et al*. [2012] due to the addition of more recent measurements and a reanalysis of the spin state of Mercury [*Margot et al*., 2012]. However, with these revised moment of inertia values, the nominal thickness of the solid outer shell of Mercury is still only slightly larger than 400 km [*Hauck et al*., 2012].

[19] In our simulations, the models run forward in time from a prescribed set of initial conditions assumed to have operated 4.5 billion years ago, presumably not long after accretion and initial differentiation of the core, mantle, and earliest crust. By definition, 4.5 Gy represents the present in these models.

3. Results

3.1. Mantle Dynamics

[20] To understand the limits on the longevity of mantle convection and the potential for magma production, we investigate the consequences of a range of silicate shell thicknesses between 300 and 600 km (Table 3). The critical Rayleigh number for the mantle scales with the core size [e.g., *Schubert et al*., 2001]. With a thin mantle, the Rayleigh number itself is reduced. However, the decrease in Rayleigh number due to the thinner mantle can be offset by other parameters, such as higher heat production, higher initial mantle temperature, or lower reference viscosities, potentially allowing supercritical Rayleigh numbers.

[21] An overview of the mode(s) of heat transport for a suite of simulations with free-slip boundary conditions at the bottom of the mantle and with variety of initial parameters (e.g., initial mantle temperature, absolute heat production, reference viscosity) is shown in Figure 2 as a function of the present core-mantle boundary temperature and the thickness of the silicate shell. Because mantle temperatures at present are the result of a broad range of parameters we, unsurprisingly, find that the mechanisms of heat transfer through the mantle in any given model are not solely related to these two model parameters. However, some general conclusions with regard to the mode of heat transfer can be made. Indeed, mantle convection is a possible mode of heat transport for all the mantle thickness values studied, and whether such convection persists to the present depends strongly, though not uniquely, on the layer thickness. In most of the cases with a mantle thickness larger than 400 km (core radius less than 2040 km), convection endures throughout the planet's history. With decreasing mantle thickness, mantle convection is possible early in Mercury's history but becomes unfavorable as the planet cools, and most models experience a cessation of convection before the present. For the smallest mantle thickness we investigated, 317 km, convection is generally a comparatively short-lived process that lasts at most 1–2.2 Gy, and no such models display active convection at present.

[22] Mantle convection is strongly controlled by both viscosity and internal heating. Because *Ra* describes the ratio of buoyancy to diffusive forces, large viscosities lead to low Rayleigh numbers, possibly inhibiting mantle convection. As for internal heating, in simulations without any internal heat sources, temperatures are not sufficiently high to maintain mantle convection for more than 2 Gy except in cases with a smaller core (Figure 3). Greater heat production leads to higher internal temperatures and lower viscosities, thus promoting more vigorous convection. However, taking an amount of internal heating close to 90% of that implied by surface abundances of K, U, and Th tends to warm the mantle so strongly as to pervasively melt the mantle at melt fractions in excess of 50%, an outcome that would suggest more voluminous magmatism than is observed. More modest values of heat production, between 25% and 50% of that indicated by surface measurements, allow mantle convection to persist for more than 2.5 Gy. Simulations with a silicate shell thickness of 317 km do not allow mantle convection for more than 2 Gy for heat production lower than 25% of the surface value.

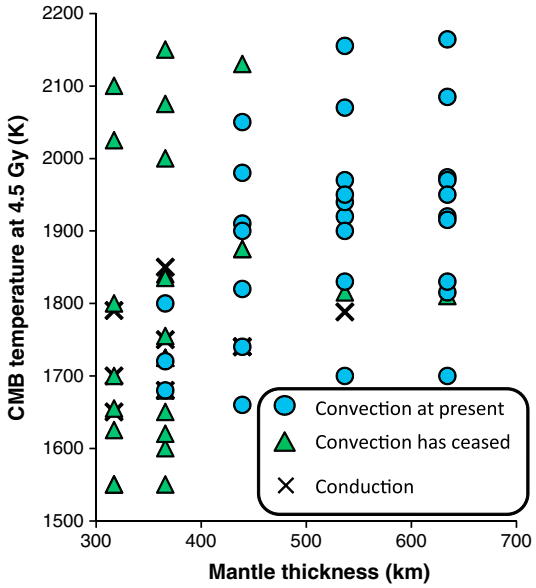

Figure 2. Mantle thermal regime for different values of mantle thickness, present CMB temperature, reference viscosities, and initial CMB temperature (cf. Table 2 and Supporting Information tables). In these simulations, free-slip boundary conditions are applied at the base of the mantle. Blue circles represent cases where mantle convection is active throughout the simulation, green triangles indicate cases for which convection ceased during model evolution and the mantle is presently stagnant and conductive, and black crosses denote cases for which the mantle never hosted convection and heat transport occurred solely by conduction.

Table 3. Relative Core Radius Adopted in the Simulations and Corresponding Values of Core Radius, Mantle Thickness, and FeS Melting Temperature[a]

r_c/r_p	r_c (km)	d (km)	T_{FeS} (K)
0.74	1806	634	1726
0.78	1903	537	1692
0.82	2001	440	1658
0.85	2074	366	1632
0.87	2123	317	1614

[a]Melting temperatures of FeS (T_{FeS}) given in the last column have been computed from the quadratic fit made by *Hauck et al*. [2006] to the observations of *Boehler* [1992] of melting temperature versus pressure.

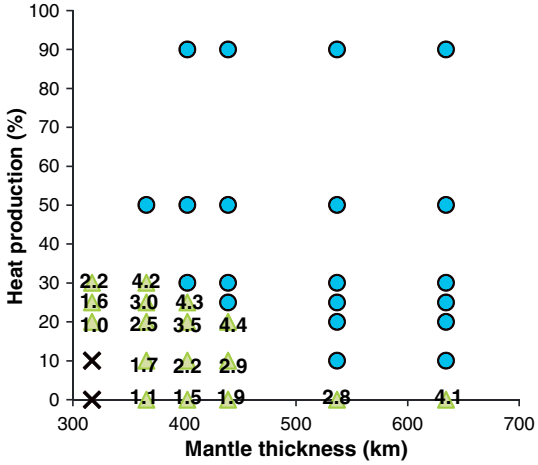

Figure 3. Mantle thermal regime for different values of mantle thickness and fraction of surface heat production. In these simulations, free-slip boundary conditions are applied at the base of the mantle. Blue circles represent cases where mantle convection is active throughout the simulation, light green triangles indicate cases for which convection ceased after the number of Gy indicated in black, and black crosses denote cases for which the mantle never convected and heat transport occurred only by conduction.

[23] An important question when considering convection near the critical Rayleigh number is whether the results have a dependence on the initial perturbation that seeds the convective motion. To address this issue, we ran cases with different perturbation amplitudes and wavelengths. Indeed, the initial pattern of convection is influenced by the initial perturbation early in the simulations, but the convective cells eventually evolve and the final planform is similar among models regardless of the initial perturbation. We also found in cases for which mantle convection ceases that the time of the shutdown of the convection is similarly unaffected by variations in the initial perturbation.

[24] A more long-term issue is the potential impact that the large variations in surface temperature on Mercury [e.g., *Vasavada et al.*, 1999] may have on the pattern and evolution of convection. Simulations with latitudinal variations in surface temperature consistent with that along a hot pole longitude [*Vasavada et al.*, 1999; *Williams et al.*, 2011] have been compared with simulations with a constant average surface temperature of 401 K. Results suggest that the pattern of surface temperatures can lead to some variations in the planform of convection [*Michel et al.*, 2011], but in general the mantle regime is only slightly affected (Figures 4 and 5). For example, Figure 4 demonstrates a modest increase in the size, and therefore a decrease in number, of the convection cells for cases in which surface temperatures are permitted to vary with latitude. We also found that the overall thermal evolution of the mantle for models is broadly similar, regardless of the surface temperature boundary conditions, although it is possible that convection may persist somewhat longer in cases with surface temperature variations (Figure 5).

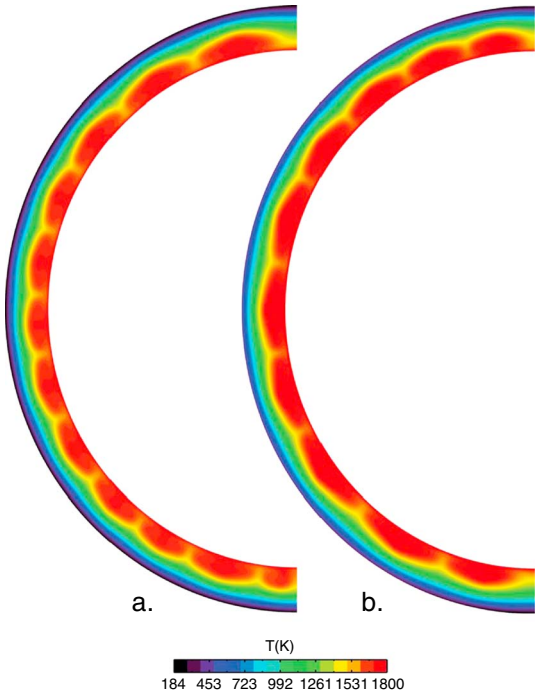

Figure 4. Snapshot of the temperature field in a 366 km thick mantle at 2.4 Gy, for two cases with mantle heat production equal to 25% of the surface value. (a) A model with constant surface temperature. (b) A model with latitudinal variation in surface temperature. In Figure 4a, the number of convective cells is greater and the cells are smaller than in Figure 4b.

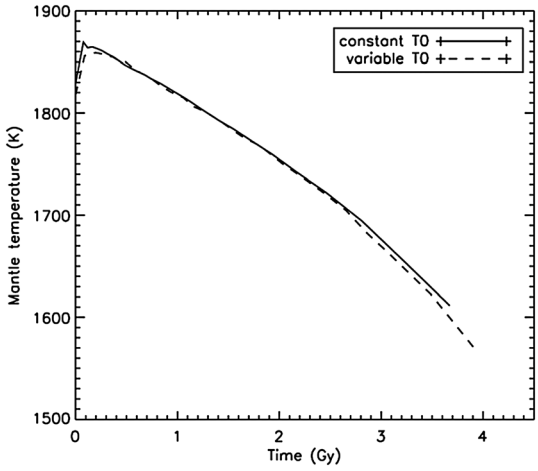

Figure 5. Average mantle temperature versus time for the simulations depicted in Figure 4. The thermal evolution is similar in both cases, although mantle convection ceases earlier in the case with constant surface temperature (solid line) than in the case with a surface temperature variation (dashed line).

3.2. No-Slip Versus Free-Slip Bottom Boundary Condition

[25] The first estimates of the Mercury's polar moment of inertia C/Mr_p^2 as well as the fractional moment of inertia of the outermost solid planetary shell C_m/C [*Smith et al.*, 2012] indicated that Mercury has a large core approximately 2030 km in radius and that the density of the solid shell

overlying the planet's liquid core is denser than would be expected given the low iron content, as well as the low Ti and comparatively low Al contents, of surface materials. From the relatively low abundance of Fe and large abundance of S at Mercury's surface as observed by MESSENGER's X-Ray Spectrometer, it has been inferred that the planet formed from chemically reduced precursory material. As noted above, this redox state tends to favor partitioning of more Si into the metal phase than under more oxidizing conditions, increasing the likelihood that Mercury's core hosts multiple light alloying elements, particularly Si and S. Such a composition will eventually result in the solidification of a layer of FeS at the top of the core, which *Smith et al*. [2012] suggest may provide an explanation for the large bulk density of the outer solid shell. However, the uncertainty in the value of C/Mr_p^2 is sufficiently large as to permit a variety of core structures with and without a solid FeS layer at the top of the core. More recent measurements of Mercury's spin state [*Margot et al*., 2012] have led to small changes in both the libration amplitude and the obliquity, leading to somewhat lower values of C/Mr_p^2 and C_m/C than previously reported. The latest moments are consistent with models both with and without a solid FeS layers at the top of the core, even for the nominal moment of inertia parameters [*Hauck et al*., 2012]. Given the reducing conditions that may govern Mercury's interior and the uncertainty in the detailed structure of Mercury's core, we investigate the implications for the mantle of cases with as well as without a solid FeS layer at the base of the mantle. Should an FeS layer be present at the base of the mantle, it would place two constraints on mantle convection: a more rigid velocity boundary condition and the requirement that present day CMB temperatures be at least below the melting temperature of FeS, which is in the range 1600–1700 K for likely CMB pressures [*Boehler*, 1992] (Table 3).

[26] Although the high-pressure shear strength of solid FeS is not yet known, it is likely to be substantially greater than that of liquid metal. Therefore, we considered a no-slip velocity boundary condition as an alternative end-member to the commonly employed free-slip condition, though the most appropriate description of the velocity condition at the core-mantle boundary may lie between these end-members. The consequence of the different boundary condition is that convection is more restricted as the velocity at the base of the mantle's lower boundary layer vanishes. The characteristics of a suite of models with a no-slip boundary condition at the base of the mantle mimic those in Figure 3, except for the different bottom boundary condition. We also considered an additional intermediate mantle layer thickness of 403 km.

[27] An overview of the suite of simulations with a no-slip velocity boundary condition at the base of the mantle and a variety of initial parameters (e.g., initial mantle temperature, absolute heat production) is illustrated in Figure 6 versus the silicate shell thickness and the CMB temperature at 4.5 Gy (present). Cases with present CMB temperatures below the FeS melting temperature are consistent with the presence of a solid FeS layer (Figure 6a). Although the no-slip boundary condition tends to reduce the vigor of mantle convection relative to otherwise equivalent cases with a free-slip lower boundary, the effect is not so strong as to prevent mantle

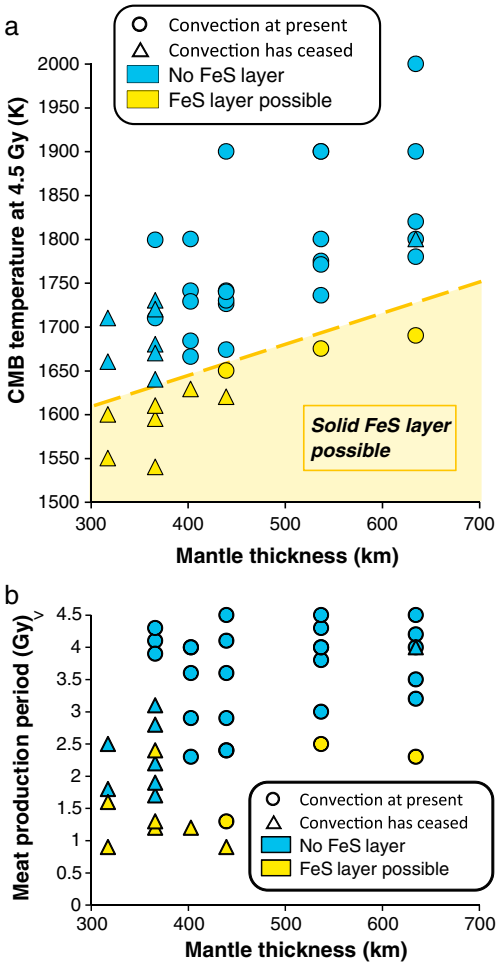

Figure 6. (a) Mantle thermal regime for different values of mantle thickness and present CMB temperature, but with a no-slip boundary condition at the base of the mantle. (b) Duration of the era of widespread magma production for the cases in Figure 6a. Melting relations are those for a mantle source volume with olivine and orthopyroxene but no clinopyroxene.

convection. Indeed, convection persisting over an extended period of time and a solid FeS layer are both possible outcomes for any of the mantle thickness values studied, though they are generally not both present at 4.5 Gy except for the cases with a greater mantle thickness. As with the free-slip cases, present mantle convection is unlikely in the cases with the smallest mantle thicknesses.

3.3. Volcanism

[28] The full nature of the source regions and degrees of melting responsible for Mercury's surface volcanic rocks has not been fully characterized. However, the inference that surface materials have average compositions that range between magnesian basalts and more ultramafic material suggests that the magmas may be products of relatively high degrees of partial melting of a low-iron peridotitic source [*Nittler et al*., 2011; *Charlier et al*., 2012; *Stockstill-Cahill et al*., 2012]. Therefore, we make the assumption that the parameterization of melting in anhydrous terrestrial peridotite derived by *Katz et al*. [2003] provides a first-order

approximation to melting in Mercury's mantle. Recent petrologic modeling suggests that clinopyroxene (cpx), which is among the first minerals to melt and is generally exhausted prior to other minerals as temperatures are raised above the solidus, may or may not be present in surface rocks with such high magnesium contents as observed on Mercury [*Stockstill-Cahill et al*., 2012]. Therefore, following the *Katz et al*. [2003] empirical parameterization for dry peridotite that has an explicit functional dependence on the cpx content of the source materials, we consider two end-members for melting of Mercury's mantle. First, we consider a cpx-free peridotite end-member [*Katz et al*., 2003], and secondly we consider a 20% modal abundance of cpx in the source material. It is worth noting that even in cases for which cpx is initially present in the mantle, as magmatism proceeds cpx will become progressively depleted until exhaustion, leading to the possibility that the cpx-free end-member may be the eventual state of the magma source regions, regardless of initial composition.

[29] The relationship between the duration of melt production and the thickness of the mantle for cases in which there is no clinopyroxene in the source region and with a no-slip bottom boundary condition is shown in Figure 6b. Over the wide range of parameters considered, partial melting in our models may be confined to the first ~1 Gy of the planet's history or may extend throughout the full 4.5 Gy. Figure 6b illustrates those specific cases for which mantle convection can be sustained to the present and a solid FeS layer is possible at the top of the modern core. Not surprisingly, the models that permit the presence of a solid FeS layer generally yield shorter melt production periods because cooler mantle temperatures are required. For cases with an extended duration of melt generation, the spatially averaged depth of shallowest melting is 200 to 300 km. Although magmatism on Mercury may have occurred as recently as 1 Ga on local scales [*Prockter et al*., 2010], the age of emplacement of the largest expanses of volcanic plains on Mercury exceeds 3.5 Ga [*Strom et al*., 2011; *Head et al*., 2011].

[30] An illustrative example of the degree of melting throughout a model is shown in Figure 7. This case shows the melt fraction at 600 My in a 400 km thick mantle with no cpx in the magma source region. In this model, mantle convection persists to the present. Although the CMB temperature at 4.5 Gy is too high to allow a solid FeS layer at the top of the modern core, mantle temperatures are sufficiently low in this model that melt production ceases after 2.5 Gy. That a number of the simulations indicate an extended interval of melt production suggests that improved constraints on the timing and erupted volumes of volcanic deposits will provide fertile ground for constraining Mercury's thermal history.

[31] To understand the potential linkage between magmas that could be produced in our models and the types of rocks inferred to be present on Mercury's surface, we calculated the degree of melting versus time for each of our models. These calculations include both of our assumed petrologic end-members: a peridotitic mantle with no clinopyroxene and one with a 20% modal abundance of clinopyroxene. We compare the maximum melt fractions, at any depth or latitude, in each of our models at two times, 100 My (4.4 Ga) and 600 My (3.9 Ga) as proxies for volcanism that may have played a role in the genesis respectively of

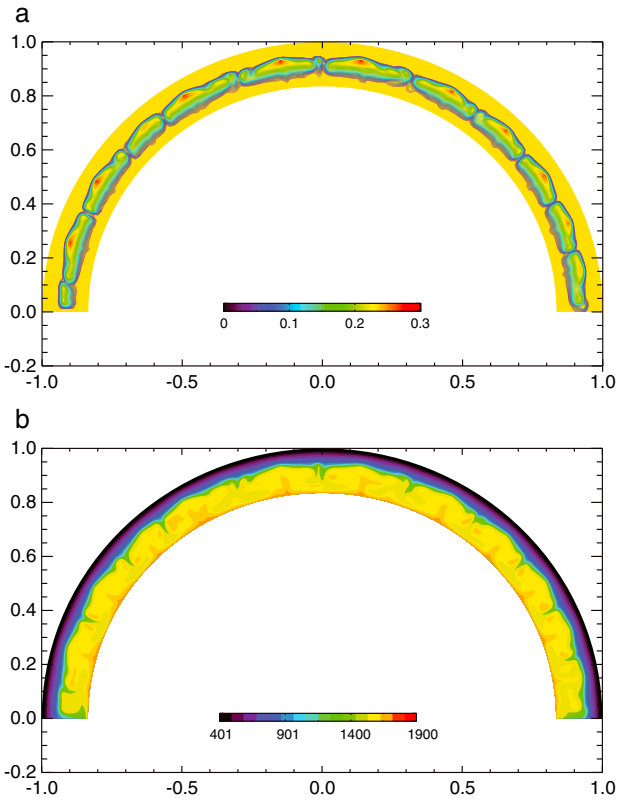

Figure 7. (a) Fractional degree of melting at 0.6 Gy for a model with a 400 km thick mantle, a heat production of 25% of the surface value, and an initial CMB temperature of 1900 K. The background color of the mantle is yellow for clarity and does not indicate any melt production. (b) Mantle temperature field for the same model and time as Figure 7a.

intercrater plains and the younger smooth plains at high northern latitudes and in association with the Caloris basin [*Strom et al*., 2011; *Head et al*., 2011; *Nittler et al*., 2011; *Weider et al*., 2012; *Stockstill-Cahill et al*., 2012]. Although such volcanism likely occurred at somewhat different times and over extended periods, these proxies give us a first look at early magma generation across a large suite of mantle evolution models and as a function of time. Figure 8a illustrates the range in the maximum melt fraction found anywhere in a given model among all cases for each mantle thickness studied. There is a wide range of possible maximum melt fractions for any given mantle thickness, with distinct differences between clinopyroxene-bearing and clinopyroxene-absent melting, particularly at the lower degrees of melting, as would be expected [e.g., *Hirschmann et al*., 1999; *Katz et al*., 2003]. Figure 8b illustrates a detailed view of the clinopyroxene-absent end-member and indicates models both with and without present mantle convection and a variety of ratios of mantle heat production to surface heat production. Multiple points with the same heat production indicate models with differing initial mantle temperatures; the higher melt fractions have temperatures of 1900 K, and the lower-melt-fraction models start at 1700 K. Models with high maximum melt fractions (e.g., >30%) are obtained for a wide range of conditions, though more consistently in

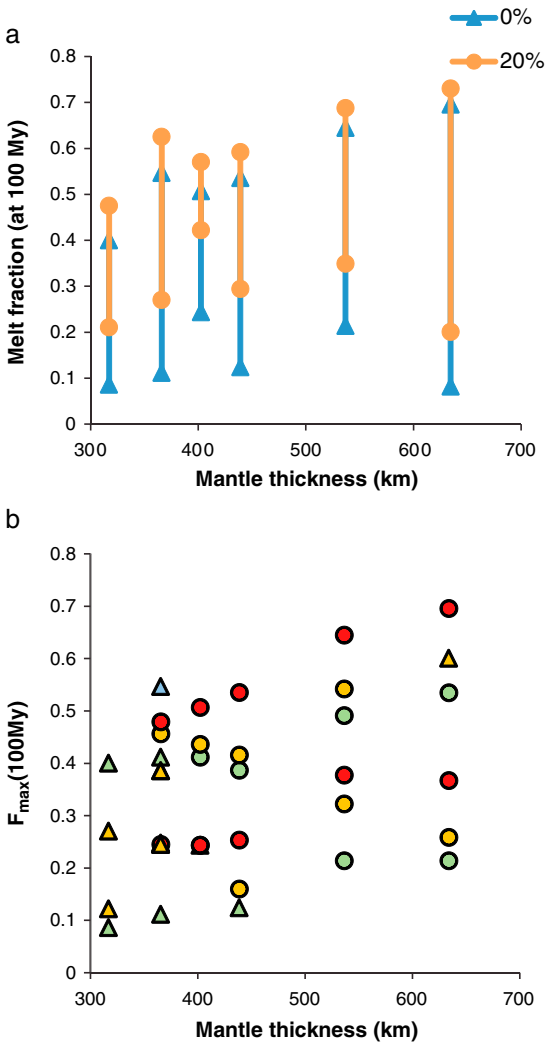

Figure 8. (a) Range of maximum degree of partial melting (F_{max}) obtained in the simulations at 100 My (4.4 Ga) as a function of the thickness of the mantle. Blue denotes models with 0% clinopyroxene (cpx) and orange with 20% cpx in the magma source. (b) Detailed view of the cpx-absent end-member at 4.4 Ga. Symbols follow the legend in Figure 2. The ratio of the modeled mantle heat production to surface heat production is represented by color. Blue represents 20%, green 25%, orange 30%, and red 50% of surface heat production.

models with higher initial temperatures. However, the addition of clinopyroxene to the magma source increases the degree of melting in all cases. In general, with initial mantle temperatures greater than 1700 K and/or modest amounts of clinopyroxene in Mercury's mantle, the production of volcanic rocks from high-degree melts of a nominally peridotitic source is possible over a wide range of conditions early in the planet's history.

[32] An important consideration for understanding the evolution of Mercury's interior is the apparent distinction between the surface compositions of the northern plains and the extensive plains associated with the Caloris basin and the compositions of older surrounding terrain characterized by generally higher Mg/Si ratios [*Nittler et al.*, 2011; *Weider et al.*, 2012; *Charlier et al.*, 2012; *Stockstill-Cahill et al.*, 2012]. It appears that both expanses of smooth plains are Calorian in age and date from a time near the end of the late heavy bombardment. Therefore, it is possible that the different compositions for the areas of heavily cratered terrain and intercrater plains that surround them may be attributable to differences in mantle temperatures, and hence partial melt fractions, between the two time periods of formation. Figure 9 indicates the change in maximum melt fraction between 4.4 and 3.9 Ga for the clinopyroxene-absent end-member. Models with the highest heat production tend to maintain or increase mantle temperature over that interval and have the potential for higher melt fractions at times appropriate to smooth plains formation, rather than less as may be indicated by X-Ray Spectrometer data [*Nittler et al.*, 2011; *Weider et al.*, 2012; *Stockstill-Cahill et al.*, 2012]. However, models with lower heat production, ≤ 30% of surface heat production, tend to show a decrease in peak melt fraction with time, potentially more consistent with observations. An important caution, however, is that in contrast with many parameterized convection calculations [e.g., *Hauck and Phillips*, 2002; *Hauck et al.*, 2004], magma production does not feed back into the energy budget or the distribution of heat production in our models. Because magma production, and the consequent concentration of radioactive elements into the crust, acts as a net loss of heat and heat production in the mantle, it is possible that initial heat production values greater than 30% of the measured surface value may be consistent with observations.

4. Discussion and Conclusion

[33] Orbital observations by the MESSENGER spacecraft bear on the history of Mercury's surface and the structure of its interior. In particular, they offer an important opportunity to improve our understanding of Mercury's internal evolution. Indeed, the inference that the solid, outermost portion of Mercury may be no more than ~400 km thick [*Smith et al.*, 2012; *Hauck et al.*, 2012], and the possibility that a portion of that solid layer may have originated as part of

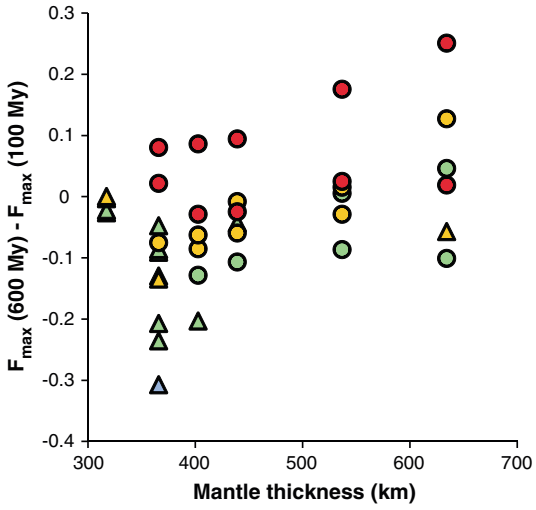

Figure 9. Change in maximum degree of partial melting between 4.4 and 3.9 Ga for the cpx-absent end-member. Legend is the same as for Figure 8b.

the core, have brought the issue of mantle convection on Mercury to the fore. Moreover, recent work has raised the possibility that volcanism associated with the Caloris basin may have been at least in part the result of dissipation of basin-forming impact heat in a contemporaneously convecting mantle [*Roberts and Barnouin*, 2012]. Our 2-D, axisymmetric model results demonstrate that mantle convection is indeed possible for at least a substantial portion of Mercury's history for even the smallest values of mantle thickness consistent with constraints on planetary interior structure. However, it is not clear whether Mercury is experiencing mantle convection at present. Should the aggregate silicate portion be less than 400 km thick, it appears difficult to sustain convection without the mantle retaining a substantial fraction of heat production relative to that of surface material.

[34] Important ancillary considerations that control the longevity of convection are the possible presence of a solid layer at the top of the core, the precipitation of solid material within the core, the fact that the planet's surface temperature is spatially variable, and the extent of magma generation early in the planet's history. The imposition of a no-slip velocity boundary condition at the base of the mantle due to an underlying solid FeS layer has a very modest impact on whether the mantle is capable of convecting at present (i.e., compare Figures 2 and 6a). However, application of a constraint on present CMB temperatures that a solid FeS layer exist at the top of the core leads to a far more limited set of conditions under which the mantle may be convecting at present. Though observations of Mercury's surface composition are consistent with a core structure that includes a solid FeS-rich layer at the top, alternative structures without such a solid layer cannot be rejected [*Smith et al*., 2012; *Hauck et al*., 2012]. Therefore, although we have considered the implications of such a solid core layer, our fundamental conclusions do not depend on its presence; however, such a layer does constrain the CMB temperature. Regardless, the process of precipitation of solid core material, whether at the top or bottom of the liquid core (or both), is important for the heat budget of the planet. We note that our models neglect the contribution of the precipitation of solids in the core heat balance due to the underconstrained composition and high-pressure phase relations of Mercury's core materials. Precipitation would provide a net increase to the heat supplied to the mantle and could act to extend the period of convection and possibly of magma generation for a given model, depending on the timing of such precipitation.

[35] An additional aspect of the question of the longevity of convection and widespread magma production is the potential role of the large variations in surface temperature. Mercury's proximity to the Sun, its eccentric orbit, and its spin-orbit resonance together give rise to large variations in surface temperature with latitude and longitude [e.g., *Vasavada et al*., 1999]. These variations include a pole-to-equator increase in surface temperature as well as a pattern of warm and hot regions that vary with longitude. Given the strength of these variations, variable surface temperatures have been investigated for their role in modulating a crustal magnetic field [*Aharonson et al*., 2004] and the thickness of the mechanical lithosphere [*Williams et al*., 2011]. Similarly, strongly variable surface temperatures affect the pattern and behavior of mantle convection (Figures 4 and 5). The effects are, understandably, more subtle than the thermal perturbations of large impacts [e.g., *Reese et al*., 2004; *Watters et al*., 2009; *Roberts and Barnouin*, 2012], but they persisted through much of Mercury's history, i.e., since Mercury was last captured into its 3:2 spin-orbit resonance. Although our axisymmetric models are capable of addressing only the latitudinal variations in surface temperature, these variations are larger than those with longitude. The longitudinal variations should nonetheless also modulate the 3-D planform of convection. Indeed, future models linking the 3-D planform of convection and its potential role in seeding the pattern of tectonic deformation [e.g., *King*, 2008] may be best served by considering whether surface temperature variations may alter the long, convective rolls observed in constant-surface-temperature, 3-D models.

[36] The large latitudinal variation in surface temperature induces pole-to-equator changes in thermal structure and hence lithospheric thickness [*Aharonson et al*., 2004], and to a lesser extent magma generation within Mercury's mantle. That the latitudinal variation may result in mantle convection persisting more than 100 My longer than the cases with constant surface temperature case is an interesting outcome. Because the extended interval constitutes only a few percent of Mercury's history, its importance for the long-term evolution of the planet is secondary to the effect of several parameters with large uncertainties, including mantle rheology and heat production. In contrast with the variation in thickness of the lithosphere, we find that at the bottom boundary there are no resolvable latitudinal variations in CMB heat flux. A consequence of such efficient convective mixing is that for a convecting mantle the surface temperature variations likely have a negligible effect on convection within Mercury's core and therefore the generation of its magnetic field. However, as a notable fraction of our models with and without surface temperature variations cease mantle convection at some point in their evolution, temperatures will conductively adjust over time and will modify CMB temperatures in pattern and in magnitude similar to surface temperatures. Furthermore, large-scale variations in the depth to the CMB, such as any related to long-wavelength variations in topography [*Zuber et al*., 2012; *Smith et al*., 2012] that depart from the axisymmetry of modeled surface temperatures, may impose an additional subtle variation in CMB temperatures in a conductive model. As spatial variations in deep mantle temperatures can affect core flow patterns [e.g., *Sumita and Olson*, 1999], these variations could be important for understanding the generation of Mercury's unusual magnetic field and its morphology [*Anderson et al*., 2011].

[37] Our calculations of magma generation for a wide range of mantle convection models demonstrate that high degrees of melting are readily obtained early in Mercury's history and that substantial evolution in peak melt fraction occurs through the era of the late heavy bombardment. These model characteristics are in line with the measured compositions of the major smooth plains deposits on Mercury and with the older and more magnesian intercrater plains [*Nittler et al*., 2011; *Weider et al*., 2012; *Charlier et al*., 2012; *Stockstill-Cahill et al*., 2012]. Generation of magma as recently as 1 Ga [*Prockter et al*., 2010] is also possible in several models, though generally in cases with higher heat production and in which convection persists to

the present. Additional constraints from MESSENGER on the history of volcanic flux on Mercury, as well as any temporal evolution in lava composition, should place strong constraints on the thermal evolution of the planet's interior.

[38] The most commonly invoked constraint on Mercury's internal evolution over the past three decades has been the limited global contraction of ~1 km in radius [*Watters et al*., 1998] inferred to have been accommodated by the planet's system of lobate scarps [e.g., *Solomon*, 1976, 1977; *Schubert et al*., 1988; *Hauck et al*., 2004; *Breuer et al*., 2007; *Zuber et al*., 2007; *Dombard and Hauck*, 2008; *Grott et al*., 2011]. Because of the limited data on high-pressure phase relationships for the Fe-Si-S system and because our models do not include the effects of phase changes in the core, we have not addressed this issue. However, MESSENGER images and altimetry have revealed a range of features that host previously unmeasured contractional strain [*Zuber et al*., 2012; *Byrne et al*., 2012; *Solomon et al*., 2012], including long-wavelength folding and large-scale systems of thrust faults. Once the magnitude and history of tectonic deformation on Mercury is better understood, further exploration of the planet's evolution with these new constraints will be warranted.

[39] Observations by the MESSENGER spacecraft in orbit about Mercury have prompted a fresh look at the thermal and dynamical evolution of the planet's interior. The comparison of a large suite of simulations of the evolution of Mercury's interior with these observations indicates that the process of mantle convection has played an important role in the planet's history despite the unusually small volume fraction of its mantle. Moreover, we find that over a wide range of conditions it is possible for Mercury's mantle to produce broadly distributed magma at degrees of melting consistent with the types of rocks inferred at its surface from geochemical measurements. Future advances in understanding the evolution of Mercury's interior will hinge on further elucidation of the volcanic and tectonic history of the planet and the constraints they provide.

[40] **Acknowledgments.** We thank the MESSENGER engineering and science teams for the development and operation of the mission and the acquisition of the first orbital data from Mercury. Scott King and an anonymous reviewer provided comments and suggestions that substantially improved this paper. This work is supported by MESSENGER Participating Scientist grant NNX07AR77G to SAH. The MESSENGER project is supported by the NASA Discovery Program under contracts NASW-00002 to the Carnegie Institution of Washington and NAS5-97271 to The Johns Hopkins University Applied Physics Laboratory. This work made use of the High Performance Computing Resource in the Core Facility for Advanced Research Computing at Case Western Reserve University.

References

Aharonson, O., M. T. Zuber, and S. C. Solomon (2004), Crustal remanence in an internally magnetized non-uniform shell: A possible source for Mercury's magnetic field?, *Earth Planet, Sci. Lett.*, *218*, 261–268, doi:10.1016/S0012-821X(03)00682-4.

Anderson, J. D., G. Colombo, P. B. Esposito, E. L. Lau, and G. B. Trager (1987), The mass, gravity field, and ephemeris of Mercury, *Icarus*, *71*, 337–349.

Anderson, B. J., C. L. Johnson, H. Korth, M. E. Purucker, R. M. Winslow, J. A. Slavin, S. C. Solomon, R. L. McNutt Jr., J. M. Raines, and T. H. Zurbuchen (2011), The global magnetic field of Mercury from MESSENGER orbital observations, *Science*, *333*, 1859–1862, doi:10.1126/science.1211001.

Balcerski, J. A., S. A. Hauck, P. Sun, II, C. Klimczak, P. K. Byrne, A. J. Dombard, O. S. Barnouin, M. T. Zuber, R. J. Phillips, and S. C. Solomon (2012), Tilted crater floors: Recording the history of Mercury's long-wavelength deformation, *Lunar Planet. Sci.*, *43*, abstract 1850.

Boehler, R. (1992), Melting of the Fe-FeO and the Fe-FeS systems at high pressure: Constraints on core temperatures, *Earth Planet. Sci. Lett.*, *111*, 217–227.

Breuer, D., S. A. Hauck II, M. Buske, M. Pauer, and T. Spohn (2007), Interior evolution of Mercury, *Space Sci. Rev.*, *132*, 229–260, doi:10.1007/s11214-007-9228-9.

Byrne, P. K., A. M. C. Şengör, C. Klimczak, S. C. Solomon, and T. R. Watters (2012), Large-scale crustal deformation on Mercury, *Lunar Planet. Sci.*, *43*, abstract 2118.

Charlier, B., T. L. Grove, and M. T. Zuber (2012), Composition and differentiation of "basalts" at the surface of Mercury, *Lunar Planet. Sci.*, *43*, abstract 1400.

Christensen, U. R. (1995), Effects of phase transitions on mantle convection, *Annu. Rev. Earth Planet. Sci.*, *23*, 65–87, doi: 10.1146/annurev.ea.23.050195.000433.

Christensen, U. R., and D. A. Yuen (1985), Layered convection induced by phase transitions, *J. Geophys. Res.*, *90*, 10,291–10,300, doi: 10.1029/JB090iB12p10291.

Davaille, A., and C. Jaupart (1994), Onset of thermal convection in fluids with temperature-dependent viscosity: Application to the oceanic mantle, *J. Geophys. Res.*, *99*, 19,853–19,866, doi:10.1029/94JB01405.

Denevi, B. W., et al. (2009), The evolution of Mercury's crust: A global perspective from MESSENGER, *Science*, *324*, 613–618.

Dombard, A. J., and S. A. Hauck II (2008), Despinning plus global contraction and the orientation of lobate scarps on Mercury: Predictions for MESSENGER, *Icarus*, *198*, 274–276, doi:10.1016/j.icarus.2008.06.008.

Grott, M., and D. Breuer (2007), The evolution of the martian elastic lithosphere and implications for crustal and mantle rheology, *Icarus*, *193*, 503–515, doi:10.1016/j.icarus.2007.08.015.

Grott, M., D. Breuer, and M. Laneuville (2011), Thermo-chemical evolution and global contraction of Mercury, *Earth Planet. Sci. Lett.*, *307*, 135–146, doi:10.1016/j.epsl.2011.04.040.

Harder, H., and G. Schubert (2001), Sulfur in Mercury's core?, *Icarus*, *151*, 118–122, doi:10.1006/icar.2001.6586.

Hauck, S. A., II, and R. J. Phillips (2002), Thermal and crustal evolution of Mars, *J. Geophys. Res.*, *107*, 5052, doi:10.1029/2001JE001801.

Hauck, S. A., II, A. J. Dombard, R. J. Phillips, and S. C. Solomon (2004), Internal and tectonic evolution of Mercury, *Earth Planet. Sci. Lett.*, *222*, 713–728, doi:10.1016/j.epsl.2004.03.037.

Hauck, S. A., II, J. M. Aurnou, and A. J. Dombard (2006), Sulfur's impact on core evolution and magnetic field generation on Ganymede, *J. Geophys. Res.*, *111*, E09008, doi:10.1029/2005JE002557.

Hauck, S. A., II, S. C. Solomon, J. -L. Margot, F. G. Lemoine, E. Mazarico, S. J. Peale, M. E. Perry, R. J. Phillips, D. E. Smith, and M. T. Zuber (2012), Mercury's internal structure as constrained by MESSENGER observations, *Lunar Planet. Sci.*, *43*, abstract 1170.

Head, J. W., et al. (2011), Flood volcanism in the northern high latitudes of Mercury revealed by MESSENGER, *Science*, *333*, 1853–1856, doi: 10.1126/science.1211997.

Hirschmann, M. M., P. D. Asimow, M. S. Ghiorso, and E. M. Stolper (1999), Calculation of peridotite partial melting from thermodynamic models of minerals and melts, III, Controls on isobaric melt production and the effect of water on melt production, *J. Petrol.*, *40*, 832–851.

Karato, S.-I., and P. Wu (1993), Rheology of the upper mantle – A synthesis, *Science*, *260*, 771–778, doi:10.1126/science.260.5109.771.

Katz, R. F., M. Spiegelman, and C. H. Langmuir (2003), A new parameterization of hydrous mantle melting, *Geochem. Geophys. Geosyst.*, *4*, 1073, doi:10.1029/2002GC000433.

King, S. D. (2008), Pattern of lobate scarps on Mercury's surface reproduced by a model of mantle convection, *Nature Geosci.*, *1*, 229–232, doi:10.1038/ngeo152.

Mackwell, S. J. (1991), High-temperature rheology of enstatite: Implications for creep in the mantle, *Geophys. Res. Lett.*, *18*, 2027–2030, doi:10.1029/91GL02492.

Malavergne, V., M. J. Toplis, S. Berthet, and J. Jones (2010), Highly reducing conditions during core formation on Mercury: Implications for internal structure and the origin of a magnetic field, *Icarus*, *206*, 199–209, doi:10.1016/j.icarus.2009.09.001.

Margot, J.-L., S. J. Peale, R. F. Jurgens, M. A. Slade, and I. V. Holin (2007), Large longitude libration of Mercury reveals a molten core, *Science*, *316*, 710–714, doi:10.1126/science.1140514.

Margot, J.-L., S. J. Peale, S. C. Solomon, S. A. Hauck, F. D. Ghigo II, R. F. Jurgens, M. Yseboodt, J. D. Giorgini, S. Padovan, and D. B. Campbell (2012), Mercury's moment of inertia from spin and gravity data, *J. Geophys. Res.*, *117*, E00L09, doi:10.1029/2012JE004161.

McCoy, T. J., T. L. Dickinson, and G. E. Lofgren (1999), Partial melting of the Indarch (EH4) meteorite: A textural, chemical, and phase relations

view of melting and melt migration, *Meteorit. Planet. Sci.*, *34*, 735–746, doi:10.1111/j.1945-5100.1999.tb01386.x.

Michel, N. C., and O. Forni (2011), Mars mantle convection: Influence of phase transitions with core cooling, *Planet. Space Sci.*, *59*, 741–748, doi:10.1016/j.pss.2011.02.013.

Michel, N. C., S. A. Hauck, C. L. Johnson, P. N. Peplowski, R. J. Phillips, and S. C. Solomon (2011), Dynamics and evolution of Mercury's interior as constrained by MESSENGER observations, Abstract P41A-1581 presented at 2011 Fall Meeting, AGU, San Francisco, Calif., 5-9 Dec.

Moresi, L.-N., and V. S. Solomatov (1995), Numerical investigation of 2D convection with extremely large viscosity variations, *Phys. Fluids*, *7*, 2154–2162, doi:10.1063/1.868465.

Nittler, L. R., et al. (2011), The major-element composition of Mercury's surface from MESSENGER X-ray spectrometry, *Science*, *333*, 1847–1950, doi: 10.1126/science.1211567.

Peplowski, P. N., et al. (2011), Radioactive elements on Mercury's surface from MESSENGER: Implications for the planet's formation and evolution, *Science*, *333*, 1850–1852, doi:10.1126/science.1211576.

Prockter, L. M., et al. (2010), Evidence for young volcanism on Mercury from the third MESSENGER flyby, *Science*, *329*, 668–671, doi:10.1126/science.1188186.

Redmond, H. L., and S. D. King (2007), Does mantle convection currently exist on Mercury?, *Phys. Earth Planet. Inter.*, *164*, 221–231, doi:10.1016/j.pepi.2007.07.004.

Reese, C. C., V. S. Solomatov, and L.-N. Moresi (1998), Heat transport efficiency for stagnant lid convection with dislocation viscosity: Application to Mars and Venus, *J. Geophys. Res.*, *103*(E6), 13,643–13,657, doi:10.1029/98JE01047.

Reese, C. C., V. S. Solomatov, J. R. Baumgardner, D. R. Stegman, and A. V. Vezolainen (2004), Magmatic evolution of impact-induced Martian mantle plumes and the origin of Tharsis, *J. Geophys. Res.*, *109*, E08009, doi:10.1029/2003JE002222.

Roberts, J. H., and O. S. Barnouin (2012), The effect of the Caloris impact on the mantle dynamics and volcanism of Mercury, *J. Geophys. Res.*, *117*, E02007, doi:10.1029/2011JE003876.

Roberts, J. H., and S. Zhong (2004), Plume-induced topography and geoid anomalies and their implications for the Tharsis rise on Mars, *J. Geophys. Res.*, *109*, E03009, doi:10.1029/2003JE002226.

Roberts, J. H., and S. Zhong (2006), Degree-1 convection in the Martian mantle and the origin of the hemispheric dichotomy, *J. Geophys. Res.*, *111*, E06013, doi:10.1029/2005JE002668.

Schubert, G., M. N. Ross, D. J. Stevenson, and T. Spohn (1988), Mercury's thermal history and the generation of its magnetic field, in *Mercury*, edited by F. Vilas, C. R. Chapman, and M. S. Matthews, pp. 429–460, University of Arizona Press, Tucson, Ariz.

Schubert, G., D. L. Turcotte, and P. Olson (2001), *Mantle Convection in the Earth and Planets*, 956 pp., Cambridge University Press, Cambridge, U.K.

Smith, D. E., et al. (2012), Gravity field and internal structure of Mercury from MESSENGER, *Science*, *336*, 214–217, doi:10.1126/science.1218809.

Solomatov, V. S. (1995), Scaling of temperature- and stress-dependent viscosity convection, *Phys. Fluids*, *7*, 266–274, doi:10.1063/1.868624.

Solomatov, V. S., and C. C. Reese (2001), Mantle convection and thermal evolution of Mercury revisited, in *Mercury: Space Environment, Surface, and Interior,* Abstract Volume, LPI Contribution 1097, pp. 92–93, Lunar and Planetary Institute, Houston, Tex.

Solomon, S. C. (1976), Some aspects of core formation in Mercury, *Icarus*, *28*, 509–521, doi:10.1016/0019-1035(76)90124-X.

Solomon, S. C. (1977), The relationship between crustal tectonics and internal evolution in the Moon and Mercury, *Phys. Earth Planet. Inter.*, *15*, 135–145, doi:10.1016/0031-9201(77)90026-7.

Solomon, S. C., et al. (2012), Long-wavelength topographic change on Mercury: Evidence and mechanisms, *Lunar Planet. Sci.*, *43*, abstract 1578.

Spohn, T., F. Sohl, K. Wieczerkowski, and V. Conzelmann (2001), The interior structure of Mercury: What we know, what we expect from BepiColombo, *Planet. Space Sci.*, *49*, 1561–1570, doi:10.1016/S0032-0633(01)00093-9.

Stevenson, D. J., T. Spohn, and G. Schubert (1983), Magnetism and thermal evolution of the terrestrial planets, *Icarus*, *54*, 466–489, doi:10.1016/0019-1035(83)90241-5.

Stockstill-Cahill, K. R., T. J. McCoy, L. R. Nittler, S. Z. Weider, and S. A. Hauck II (2012), Magnesium-rich crustal compositions on Mercury: Implications for magmatism from petrologic modeling, *J. Geophys. Res.*, *117*, E00L15, doi:10.1029/2012JE004140.

Strom, R. G., M. E. Banks, C. R. Chapman, C. I. Fassett, J. A. Forde, J. W. Head III, W. J. Merline, L. M. Prockter, and S. C. Solomon (2011), Mercury crater statistics from MESSENGER flybys: Implications for stratigraphy and resurfacing history, *Planet. Space Sci.*, *59*, 1960–1976.

Sumita, I., and P. Olson (1999), A laboratory model for convection in Earth's core driven by a thermally heterogeneous mantle, *Science*, *286*, 1547–1549, doi:10.1126/science.286.5444.1547.

Turcotte, D. L., and G. Schubert (2002), *Geodynamics*, 472 pp. 2nd ed., Cambridge University Press, Cambridge.

Van Hoolst, T., F. Sohl, I. Holin, O. Verhoeven, V. Dehant, and T. Spohn (2007), Mercury's interior structure, rotation, and tides, *Space Sci. Rev.*, *132*, 203–227, doi:10.1007/s11214-007-9202-6.

Vasavada, A. R., D. A. Paige, and S. E. Wood (1999), Near-surface temperatures on Mercury and the Moon and the stability of polar ice deposits, *Icarus*, *141*, 179–193, doi:10.1006/icar.1999.6175.

Watters, T. R., M. S. Robinson, and A. C. Cook (1998), Topography of lobate scarps on Mercury: New constraints on the planet's contraction, *Geology*, *26*, 991–994, doi:10.1130/0091-7613/1998/026.

Watters, W. A., M. T. Zuber, and B. H. Hager (2009), Thermal perturbations caused by large impacts and consequences for mantle convection, *J. Geophys. Res.*, *114*, E02001, doi:10.1029/2007JE002964.

Weider, S. Z., L. R. Nittler, R. D. Starr, T. J. McCoy, K. R. Stockstill-Cahill, P. K. Byrne, B. W. Denevi, J. W. Head, and S. C. Solomon (2012), Chemical heterogeneity on Mercury's surface revealed by the MESSENGER X-Ray Spectrometer, *J. Geophys. Res.*, *117*, E00L05, doi:10.1029/2012JE004153.

Williams, J.-P., O. Aharonson, and F. Nimmo (2007), Powering Mercury's dynamo, *Geophys. Res. Lett.*, *34*, L21201, doi:10.1029/2007GL031164.

Williams, J.-P., J. Ruiz, M. A. Rosenburg, O. Aharonson, and R. J. Phillips (2011), Insolation driven variations of Mercury's lithospheric strength, *J. Geophys. Res.*, *116*, E01008, doi:10.1029/2010JE003655.

Zhong, S., M. T. Zuber, L. Moresi, and M. Gurnis (2000), Role of temperature dependent viscosity and surface plates in spherical shell models of mantle convection, *J. Geophys. Res.*, *105*, 11,063–11,082, doi:10.1029/2000JB900003.

Zuber, M. T., et al. (2007), The geophysics of Mercury: Current status and anticipated insights from the MESSENGER mission, *Space Sci. Rev.*, *131*, 105–132, doi:10.1007/s11214-007-9265-4.

Zuber, M. T., et al. (2012), Topography of the northern hemisphere of Mercury from MESSENGER laser altimetry, *Science*, *336*, 217–220, doi:10.1126/science.1218805.